Physics – Uspekhi **65** (12) 1290 – 1302 (2022)

REVIEWS OF TOPICAL PROBLEMS PACS numbers: 07.60.Vg, **42.25. – p**, 42.81.Pa

Tilted fiber Bragg gratings and their sensing applications

O V Butov, K A Tomyshev, I A Nechepurenko, A V Dorofeenko, S A Nikitov

DOI: https://doi.org/10.3367/UFNe.2021.09.039070

Contents

Abstract. The review covers current achievements and prospects for the development of fiber sensorics associated with tilted fiber Bragg gratings (TFBGs), including metal-coated (plasmonic) sensors. The physical nature of the excitation of the cladding modes in such structures is discussed, and the main properties of TFBGs are considered. Special attention is devoted to sensing applications of TFBGs, including data processing methods for TFBG sensing systems. The process of fabricating tilted fiber Bragg gratings is described, as is the method of thin metal film deposition onto the side surface of the fiber.

Keywords: tilted fiber Bragg grating, optical fiber sensor, surface plasmon resonance, coupled mode theory, data processing

1. Introduction

The origin of the fiber optics era can be traced to the early 1970s, when the first low-loss silica fiber was developed, which gave a strong impetus to the development of optical communication [1]. Today, the use of fiber-optic technologies goes far beyond this area [2]. New types of optical fibers and devices based on them are being created [3–7]. Fiber sensing [8–12] and laser physics [13–22] are actively being developed based on optical fibers. The impetus for the development of these areas, among other things, the discovery in 1978 of photosensitivity of optical fibers, i.e., the possibility of a permanent change in the refractive index of some doped silica glasses, which mainly form the core of fiber optical waveguides under the action of high-energy optical radiation. The effect was first discovered when trying to transmit laser radiation in the visible range through an optical fiber [23]. During a long exposure, the fiber ceased to transmit light at a given wavelength, while remaining transparent at other wavelengths. The reason for this phenomenon was the formation of a standing wave in the fiber as a result of the interference of the wave reflected from the end face of the fiber with the incident laser radiation. The reflected wave formed a grating in the fiber with a period equal to half the wavelength, which led to resonant reflection. Subsequently, the structure was called a fiber Bragg grating (FBG) by analogy with the Bragg–Wulff effect [14, 24].

Later, it was shown that the most efficient inscription of Bragg gratings occurs when exposing the fiber to laser radiation in the ultraviolet (UV) range, which coincides with the absorption bands of impurity defects in the doped core, and methods for fabricating Bragg gratings with side irradiation were developed [25]. To create the necessary periodic structure, an interference pattern was formed in the core of an optical fiber exposed to a UV laser beam using interferometers or phase masks [14, 26–28]. The advantage of this method consists in the formation of an efficient Bragg grating in a short section of the fiber and in the possibility of inscribing a grating with the required period value by changing the convergence angle of the interferometer beams or applying a phase mask with a different period.

Bragg gratings are used as narrow-band optical filters, e.g., to select optical channels [14, 29], as mirrors of fiber laser resonators [13–21], and as sensors of physical quantities

O V Butov [1, a], **K A Tomyshev** [1, b], **I A Nechepurenko** [1, 2, c], **A V Dorofeenko** [1, 2, 3, d], **S A Nikitov** [1, 4, 5, e]
[1] Kotelnikov Institute of Radioengineering and Electronics, Russian Academy of Sciences, ul. Mokhovaya 11, str. 7, 125009 Moscow, Russian Federation
[2] Dukhov Research Institute of Automatics, ul. Sushchevskaya 22, 127030 Moscow, Russian Federation
[3] Institute for Theoretical and Applied Electrodynamics, Russian Academy of Sciences, ul. Izhorskaya 13, 125412 Moscow, Russian Federation
[4] Moscow Institute of Physics and Technology (National Research University), Institutskii per. 9, 141701 Dolgoprudnyi, Moscow region, Russian Federation
[5] Chernyshevskii Saratov State University, ul. Astrakhanskaya 83, 410012 Saratov, Russian Federation
E-mail: [a] obutov@mail.ru, [b] scatterdice@gmail.com, [c] nechepurenko@phystech.edu, [d] adorofeenko@itae.ru, [e] nikitov@cplire.ru

Received 25 June 2021, revised 16 September 2021
Uspekhi Fizicheskikh Nauk **192** (12) 1385 – 1398 (2022)
Translated by V L Derbov

[2, 30–37]. Indeed, under external action, such as longitudinal mechanical stress or heating, the optical properties of the fiber structure change, which leads to a change in the Bragg reflection wavelength.

Thus, the creation of fiber Bragg gratings marked the beginning of a new major direction in applied science. Currently, sensors based on Bragg gratings are widely used in various industries to monitor key technological parameters, the state of structural elements, and complex engineering structures in a number of applications replacing electrical counterparts.

Worth special attention are Bragg gratings, in which the grating planes are tilted by a certain angle with respect to the cross section of the optical fiber. Such structures are called tilted fiber Bragg gratings (TFBGs). Interest in such structures is associated with their ability to excite cladding modes [38].

The discovery of TFBGs can be traced back to the 1990s [39–42], when 'classical' Bragg gratings with layers of the refractive index modulation pattern orthogonal to the fiber axis were actively studied, the technology for their production was developed, and the range of problems solved with them was expanding. A mathematical description of TFBG operation principles was proposed in 1996 [41] and then generalized in 2000–2001 [43, 44], which gave rise to the beginning of numerous research developments. Soon, attempts were made to use TFBGs to solve various problems, such as spectral filtering [42], measuring optical signal polarization [45, 46], and polarization loss compensation [47]. Sensing applications of TFBGs are of particular practical interest due to the ability of cladding modes to interact with the fiber environment [48–61].

The present review considers the properties, principles of operation, and methods for fabricating tilted Bragg gratings, as well as sensors based on them and mathematical methods for processing the results obtained.

2. Theory of optical fibers with tilted Bragg gratings

2.1 Mode coupling via a tilted Bragg grating

Fiber Bragg gratings are a widespread type of fiber elements. There are many types of Bragg gratings, namely, gratings with a constant period and variable one (chirped), and gratings with refractive index modulation intensity varying along the fiber axis (apodized) [62]. However, in most cases, what is referred to is periodic fiber gratings with grating planes arranged uniformly along the fiber and strictly perpendicular to the fiber axis. The structure of such a Bragg grating is shown schematically in Fig. 1.

A specific feature of the Bragg grating is the ability to reflect light in a limited spectral range, called the band gap. The band gap spectral position is described by the Bragg–Wulff [63] law, according to which the resonant (Bragg) wavelength λ_B depends on the grating period Λ and the effective refractive index $n_c^{\text{eff}} = ck_c/\omega$ of the fundamental mode propagating through the fiber core (the respective variables are labelled by the subscript 'c'):

$$\lambda_B = n_c^{\text{eff}} 2\Lambda . \qquad (1)$$

Figure 2 schematically presents the dispersion curves for various modes of an optical fiber, including the cladding modes that propagate in the fiber cladding. It is worth noting

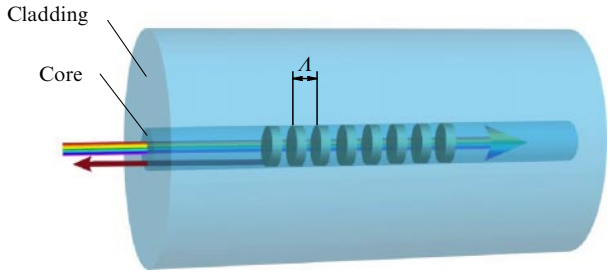

Figure 1. Schematic image of the structure of an optical fiber with nontilted FBG.

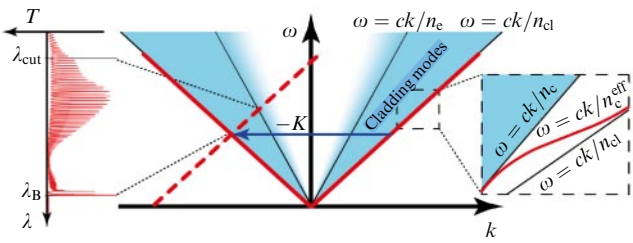

Figure 2. Mode coupling in terms of dispersion curves. Dispersion curves of the core are shown in red. Blue regions contain the dispersion curves of cladding modes; light blue denotes cladding mode leakage into the external space.

that the fundamental mode propagates through the core and is reflected from the cladding; therefore, its effective refractive index is between those of the core (n_c) and the cladding (n_{cl}) materials: $n_c < n_c^{\text{eff}} < n_{cl}$. This inequality means that the dispersion curve of the fundamental mode is located between the light cones $\omega = ck/n_c$ and $\omega = ck/n_{cl}$ corresponding to the materials of the core and the cladding. In most standard optical fibers, the refractive indices of the core and the cladding are close and, therefore, the dispersion curve of the fundamental mode is clamped between the close cones (see the inset in Fig. 2).

The cladding modes propagate in the core and in the cladding but experience total internal reflection from the external medium with the refractive index n_e. Therefore, their dispersion curves are between the light cones corresponding to the external medium and the glass. Because of the large diameter of the cladding (125 μm for standard fibers), the dispersion curves of the cladding modes are arranged very densely and, in fact, fill the painted region in Fig. 2. Such an approximation agrees with the picture of geometric optics, in which the modes are considered rays travelling along different paths inside the cladding. However, such a picture provides a strongly limited description of the system, since, in the transmission spectra of Bragg gratings, the result of coupling the fundamental (core) mode to *individual* cladding modes is clearly seen. This discreteness cannot be explained in terms of geometric optics.

The coupling of fiber modes via the Bragg grating is conveniently explained in terms of wavenumbers. By a wavenumber, we mean the projection of the wave vector onto the fiber axis. We will consider only this projection, since in an optical waveguide the radial (i.e., perpendicular to the axis) projection is indefinite. The Bragg grating diffraction is efficient only if the phase matching condition is valid, when the wave numbers of the coupled modes differ by an integer number of reciprocal grating constants $K = 2\pi/\Lambda$. This

quantity is obviously independent of the refractive index and is determined solely by the grating geometry and, therefore, it is possible to separate different kinds of couplings of fiber modes via the grating [48]. The classical Bragg reflection occurs when the wave numbers of the incident and reflected waves are equal in magnitude and have opposite directions, and the Bragg scattering converts one wave into another, $k_c - K = -k_c$, from which the Bragg condition follows. The corresponding frequency is marked by a horizontal arrow in Fig. 2.

When the incident radiation wavelength is greater than the Bragg one, $\lambda > \lambda_B$, the core mode does not couple to any other modes via the grating. Indeed, the fundamental mode dispersion curve translated by a reciprocal grating constant (dashed line in Fig. 2) does not cross the dispersion curves of other modes below the Bragg resonance frequency, marked by a horizontal arrow. As a result, at the mentioned wavelength, no fundamental mode scattering occurs.

At wavelengths below the Bragg one, $\lambda < \lambda_B$, the dashed line in Fig. 2 crosses the dispersion curves of the cladding modes, so that these modes can get excited at the expense of Bragg grating diffraction. The wavelength range is bounded from below by the cut-off condition $\lambda > \lambda_{cut}$, corresponding to the leakage of the cladding mode field into the environment. Nevertheless, even in the region $\lambda < \lambda_{cut}$, a limited number of near-cut-off cladding modes are characterized by sufficiently slow leakage (light blue region in Fig. 2) and can interact with the core mode. As can be seen from Fig. 2, the cut-off wavelength can be calculated from the relation $\lambda_{cut} = \lambda_B(n_e + n_c)/(2n_c)$ (in the calculations, it is assumed that $n_c = 1.448$ [64], $n_e = 1.317$ for water [65]). Note, however, that in the classical (nontilted) Bragg grating (Fig. 1), the grating planes are perpendicular to the waveguide axis, and no efficient excitation of cladding modes occurs (for more details, please see Section 2.3).

Efficient excitation of cladding modes is implemented using a tilted fiber Bragg grating. In a TFBG, the normal vector to the grating plane is directed at a certain angle to the fiber axis (Fig. 3). It is intuitively clear that the tilt of the grating causes scattering from the core to the cladding; however, such a conclusion is based on the mirror reflection concept within geometric optics. From the point of view of wave optics, the phase matching condition has to be fulfilled to ensure the coupling of core and cladding modes. This condition holds with high accuracy only in the longitudinal direction of the fiber, in which the refractive index modulation pattern has many repeated layers. In the transverse section, the refractive index modulation pattern has only a few cycles, which is not enough to ensure the phase matching condition for radial wave numbers. In terms of geometric optics, this corresponds to the possibility of reflection from the tilted grating planes at various angles (see Fig. 3). In terms of wave optics, the tilt of the grating leads to an increase in the transverse overlap integral of the core mode and the cladding ones (see Section 2.3 for more detail).

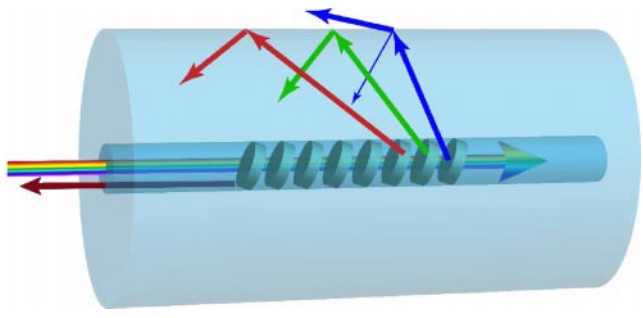

Figure 3. Schematic representation of the optical fiber structure with tilted FBG and the process of fundamental mode scattering. Wavelengths are symbolically indicated by color: red for longer wavelengths, blue for shorter wavelengths. The arrow outside the fiber indicates leakage.

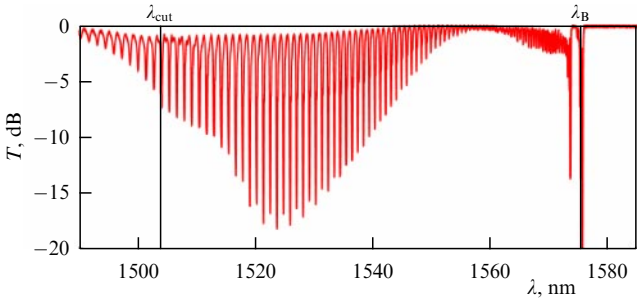

Figure 4. Experimental TFBG transmission spectra for a fiber merged in water. Vertical lines show the wavelengths corresponding to resonance Bragg scattering (λ_B) and cut-off (λ_{cut}). The data were obtained by the authors.

When changing the wavelength, the phase matching condition in the longitudinal direction, $k - K = -k_{cl}$, is fulfilled for cladding modes with the wave number k_{cl}. As a result, the TFBG transmission spectrum has dips at wavelengths corresponding to the excitation of these cladding modes. Figure 4 shows an example of a typical spectrum of a TFBG immersed in water.[1] The main peak of Bragg reflection is seen in the right-hand part of the spectrum (the wavelength λ_B), the remaining peaks corresponding to cladding modes. The cladding modes that find themselves in the light cone $\omega = ck/n_e$ leak to the surrounding space. As a result, in the region $\lambda < \lambda_{cut}$, the peak amplitudes sharply decrease.

The leakage condition and, consequently, the cut-off wavelength λ_{cut} depend on the surrounding refractive index. Moreover, even the cladding modes far from the leakage condition possess an evanescent field in the external medium around the fiber, which makes their wave numbers dependent on the refractive index of this external medium. Thus, upon a change in the refractive index, a shift in the cut-off wavelength λ_{cut} is observed in the TFBG spectrum, and the frequencies of cladding resonances are displaced. This TFBG property is used to create refractive index sensors [48, 51, 55–61].

Practical applications of tilted gratings in sensorics are associated with the use of functional coatings. Such coatings are applied to the optical waveguide surface, making it possible to transform the change in external factors into a change in the refractive index of the immediate environment of the fiber. For example, the functionalization of the surface with antibodies and/or aptamers allows fabricating

[1] The grating is inscribed in a standard telecommunication Corning CSMF-28 fiber by means of phase mask technology. An ArF excimer laser with a wavelength of 193 nm was used. The mask period was 1088 nm, the exposure time was about 5 min. The fiber was preliminarily saturated with hydrogen at a pressure of 100 atm and a temperature of 90 °C for 49 hours. The tilt angle of the grating planes that determines the number and spectral position of the cladding mode peaks was 11.7°.

TFBG-based biosensors [66]. In this case, the functional coating ensures the binding of a biological analyte to the sensor surface. Other examples of using functional coatings are the sensors of relative humidity [52, 67, 68], which use coatings of hygroscopic materials, and a pH-sensor with a polyaniline coating [69]. In both cases, the refractive index of the coating itself changes with the change in the measured medium parameter, which is detected by the grating.

2.2 Mode coupling in the presence of a metal coating

To further increase the resolution of TFBG-based sensors, the effect of plasmon resonance is used. Surface plasmon polaritons are surface waves propagating along a metal/dielectric interface [70–73]. The plasmon wave number substantially depends on the dielectric constants of the materials, separated by the interface at which the plasmon is excited. For an electromagnetic wave satisfying the condition of phase matching (i.e., closeness of wave numbers) with the plasmon, the effect of plasmon resonance is observed, accompanied by a sharp increase in metal absorption. The classic scheme for exciting plasmon resonance is the Kretschmann configuration (Fig. 5a) [74–78], in which the frequency or angular reflection spectrum of a thin (30–50 nm) metal film is measured for a beam incident through a prism. In the reflection spectrum, the plasmon resonance is observed as a sharp increase in the absorption ('frustrated total internal reflection') (Fig. 5b).

Surface plasmon resonance in planar structures is widely used in various fields of modern science and technology. The high sensitivity of the surface resonance wavelength to changes in the refractive index of the dielectric medium (Fig. 5b) was a prerequisite for the creation of highly sensitive sensors [79, 80]. Functionalization of the metal surface with biological objects allowed creating measuring complexes for biomedical applications [81, 82].

By analogy with layered systems, the deposition of a metal coating on the surface of an optical fiber can create conditions for the excitation of plasmon resonance. To match the wave numbers of the fiber mode and the plasmon, various fiber schemes are used. Most of them require a change in the fiber geometry, including side polishing, etching and thermal redrawing [49, 84–89], fiber insets [49, 90, 91], excitation of plasmons at an end face of the fiber [49, 92–95], and fiber bending [49, 91, 96].

For practical applications, of particular interest are plasmonic sensors that do not require changing the fiber geometry. This possibility is realized in sensors based on tilted Bragg gratings coated with a thin metal layer [50, 97–108] (Fig. 6). As was mentioned above, a TFBG ensures the excitation of a series of cladding modes. In the geometric optics approximation, the rays scattered by the TFBG are incident on the fiber/metal film interface at different angles. Such a system is, in essence, a fiber analog of the Kretschmann configuration (see Fig. 6). Strictly speaking, the dispersion curve of the plasmon, whose field is localized at the metal/environment interface, is located in the same region as the dispersion curves for cladding modes (Fig. 7, dotted line). The wave number matching of the cladding modes and the plasmon mode leads to their hybridization and, consequently, to a steep drop in the intensity of the relevant cladding modes. Due to an increase in the imaginary part of the wave number, such modes cease to be coupled to the fundamental mode, and a characteristic constriction appears

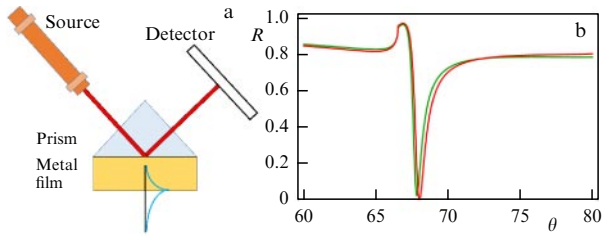

Figure 5. Kretschmann's configuration: geometry (a) and characteristic dependence of the reflection coefficient R on the incidence angle θ (angular spectrum) and its displacement upon a change in the refractive index (b) [83].

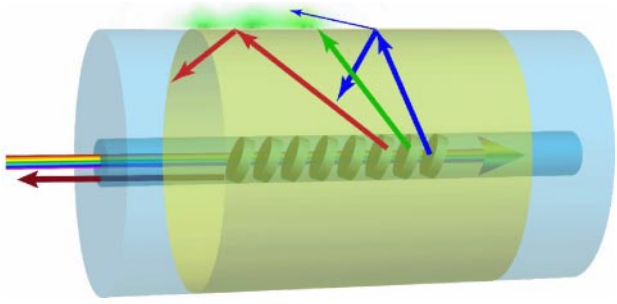

Figure 6. Principle of exciting surface plasmon polaritons by means of a TFBG and the process of fundamental mode scattering. Color is used to symbolically indicate wavelength: red for longer waves and blue for shorter waves. Green cloud outside the fiber represents the surface plasmon polariton.

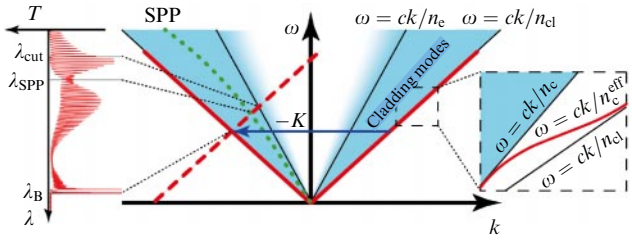

Figure 7. Mode coupling in terms of dispersion curves. Red lines show dispersion curves for the core. In blue regions are dispersion curves for cladding modes; light blue color means leakage of cladding modes to the external space. Dotted green line shows the dispersion curve for the surface plasmon polariton (SPP).

in the transmission spectrum (Fig. 8) [49, 109]. The constriction arises only in the scattering of a P-polarized wave, while the S-polarized one does not couple to the plasmon (Fig. 8a). In this case, S- and P-polarizations are determined by the direction of the electric field vectors, perpendicular and parallel, respectively, to the waveguide longitudinal section plane in which the scattering is observed.

Thanks to the dependence of the plasmon wave number on the refractive index of the surrounding medium, the fiber with a TFBG and plasmonic coating appears to be a sensitive sensor of the surrounding refractive index (Fig. 8b). As a rule, plasmonic TFBG-based sensors demonstrate an order of magnitude higher resolution than do nonplasmonic counterparts due to the more distinctly expressed resonance in the spectrum [100, 109, 110], which makes them especially promising for use in immunoassay and high-precision physicochemical measurements.

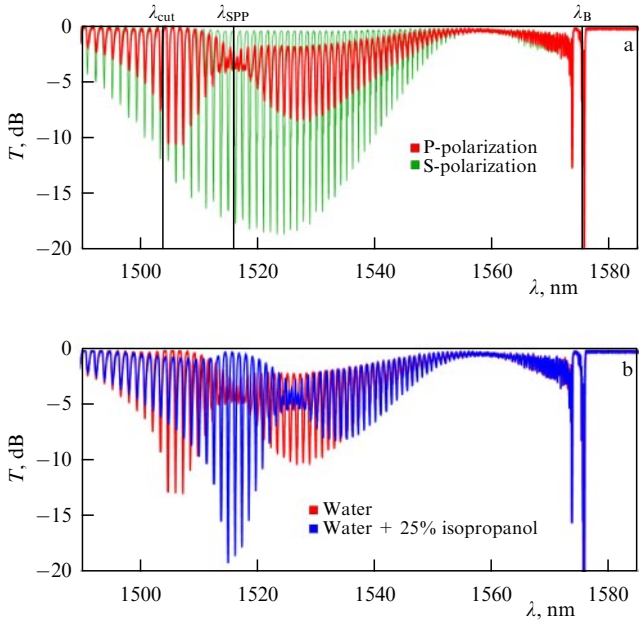

Figure 8. Experimental TFBG transmission spectra: (a) for the scattering of waves with different polarizations, 'plasmonic' (P) and 'nonplasmonic' (S), on a titled grating; (b) for the scattering of a P-polarized wave in a fiber merged in pure water and 25% aqueous solution of isopropanol. Vertical lines indicate wavelengths corresponding to the resonance Bragg reflection (λ_B), surface plasmon (λ_{SPP}), and cut-off (λ_{cut}). The data were obtained by the authors.

2.3 Coupled mode theory for calculating the transmission spectra of fibers with tilted Bragg gratings

The most common method of theoretically describing waves in fibers with Bragg gratings is the coupled mode theory, which allows formulating a system of differential equations for the mode amplitudes in a fiber, 'unperturbed' by the grating [111, 112]. In this approach, the electric and magnetic field distributions $\mathbf{e}_n(r,\varphi)\exp(\mathrm{i}k_n z)$ and $\mathbf{h}_n(r,\varphi)\exp(\mathrm{i}k_n z)$ in the modes are assumed to be known, where the functions $\mathbf{e}_n(r,\varphi)$ and $\mathbf{h}_n(r,\varphi)$ describe the transverse distributions of the fields, and k_n is the wave number of the nth mode determining the field variation along the fiber axis z. The total fields obey the Maxwell equations

$$\nabla\times\mathbf{E}=\mathrm{i}k_0\mathbf{H}\,, \tag{2}$$

$$\nabla\times\mathbf{H}=-\mathrm{i}k_0\big(\varepsilon(r)+\delta\varepsilon(\mathbf{r})\big)\mathbf{E}\,, \tag{3}$$

where $\varepsilon(r)$ is the distribution of permittivity in the fiber without grating, $\delta\varepsilon(\mathbf{r})$ is the permittivity perturbation that describes the Bragg grating (straight or tilted), and $k_0=\omega/c$ is the wave number in free space. Let us expand the field in the fiber with the grating in terms of the modes

$$\mathbf{E}=\sum_n a_n(z)\,\mathbf{e}_n(r,\varphi)\exp(\mathrm{i}k_n z)\,, \tag{4}$$

$$\mathbf{H}=\sum_n a_n(z)\,\mathbf{h}_n(r,\varphi)\exp(\mathrm{i}k_n z)\,, \tag{5}$$

where the dependence $a_n(z)$ is caused by the presence of the perturbation $\delta\varepsilon(\mathbf{r})$. Since the mode fields obey the 'unperturbed' Maxwell equations,

$$\nabla\times\big(\mathbf{e}_n\exp(\mathrm{i}k_n z)\big)=\mathrm{i}k_0\mathbf{h}_n\exp(\mathrm{i}k_n z)\,, \tag{6}$$

$$\nabla\times\big(\mathbf{h}_n\exp(\mathrm{i}k_n z)\big)=-\mathrm{i}k_0\varepsilon(r)\,\mathbf{e}_n\exp(\mathrm{i}k_n z)\,, \tag{7}$$

when substituting expansions (4), (5) into Eqns (2), (3), all terms are mutually cancelled except those containing the perturbation $\delta\varepsilon(\mathbf{r})$ and the spatial derivatives of the amplitudes $a_n(z)$:

$$\sum_n \nabla a_n(z)\times\mathbf{e}_n(r)\exp(\mathrm{i}k_n z)=0\,, \tag{8}$$

$$\sum_n \nabla a_n(z)\times\mathbf{h}_n(r)\exp(\mathrm{i}k_n z) = -\mathrm{i}k_0\delta\varepsilon(\mathbf{r})\sum_n a_n(z)\,\mathbf{e}_n(r)\exp(\mathrm{i}k_n z)\,. \tag{9}$$

To derive an equation for the mode amplitude $a_m(z)$ with a certain number m, we make use of the orthogonality of modes, which is expressed by the relation [113]

$$\int(\mathbf{e}_n\times\mathbf{h}_m^*+\mathbf{e}_m^*\times\mathbf{h}_n)\,\mathrm{d}\mathbf{S}=0\,, \tag{10}$$

where the integral is over the cross section, and the vector area element $\mathrm{d}\mathbf{S}$ is oriented along the fiber axis. Let us perform a scalar product of both sides of Eqn (8) by $\mathbf{h}_m^*$ and of both sides of Eqn (9) by $\mathbf{e}_m^*$ and find the difference of the resulting equations. A cyclic change of vectors in the mixed products yields

$$\sum_n \nabla a_n(z)(\mathbf{e}_n\times\mathbf{h}_m^*)+\sum_n \nabla a_n(z)(\mathbf{e}_m^*\times\mathbf{h}_n)\exp(\mathrm{i}k_n z) = \mathrm{i}k_0\delta\varepsilon(\mathbf{r})\sum_n a_n(z)\,\mathbf{e}_m^*\mathbf{e}_n\exp(\mathrm{i}k_n z)\,. \tag{11}$$

Let us integrate both sides of Eqn (11) over the cross section and take into account that $\mathrm{d}S\nabla a_n(z)=\mathrm{d}\mathbf{S}(\mathrm{d}a_n/\mathrm{d}z)$. Due to the orthogonality condition (10), on the left-hand side of the obtained equation only one term corresponding to $n=m$ remains:

$$\frac{\mathrm{d}a_m}{\mathrm{d}z}\int(\mathbf{e}_m\times\mathbf{h}_m^*+\mathbf{e}_m^*\times\mathbf{h}_m)\,\mathrm{d}\mathbf{S} = \mathrm{i}k_0\sum_n a_n(z)\left[\int\delta\varepsilon(\mathbf{r})(\mathbf{e}_m^*\mathbf{e}_n)\,\mathrm{d}S\right]\exp\big[\mathrm{i}(k_n-k_m)z\big]\,. \tag{12}$$

Note that on the left-hand side of the equation the flow of energy transferred by the mode has been obtained,

$$J_m=\frac{c}{16\pi}\int(\mathbf{e}_m\times\mathbf{h}_m^*+\mathbf{e}_m^*\times\mathbf{h}_m)\,\mathrm{d}\mathbf{S}\,, \tag{13}$$

which will be used as a norm. Let us denote the coefficient of mode coupling as

$$w_{mn}=\frac{1}{8\pi}\int\delta\varepsilon(\mathbf{r})(\mathbf{e}_m^*\mathbf{e}_n)\,\mathrm{d}S\,. \tag{14}$$

We arrive at a system of equations for the amplitudes of coupled modes in the waveguide:

$$J_m\frac{\mathrm{d}a_m}{\mathrm{d}z}=\frac{\mathrm{i}ck_0}{2}\sum_n w_{mn}a_n(z)\exp\big[\mathrm{i}(k_n-k_m)z\big]\,. \tag{15}$$

The fiber Bragg grating corresponds to a small perturbation of the permittivity, which is periodic along the fiber axis with the period Λ: $\delta\varepsilon(\mathbf{r})=\sum_{l=-\infty}^{+\infty}\varepsilon_l(x,y)\exp(\mathrm{i}Klz)$, where $K=2\pi/\Lambda$ is the reciprocal grating constant. Then, the coupling coefficient takes the form $w_{mn}=\sum_{l=-\infty}^{+\infty}v_{lmn}\exp(\mathrm{i}Klz)/(8\pi)$,

where the transverse overlap of the mth and nth modes via the lth component of Bragg grating permittivity is denoted as

$$v_{lmn} = \int \varepsilon_l \left(\mathbf{e}_m^* \mathbf{e}_n\right) \mathrm{d}S . \tag{16}$$

It follows that

$$J_m \frac{\mathrm{d}a_m}{\mathrm{d}z} = \frac{\mathrm{i}ck_0}{2} \sum_n a_n(z) \sum_{l=-\infty}^{+\infty} v_{lmn} \exp\left[\mathrm{i}(k_n - k_m + Kl)z\right] . \tag{17}$$

For low-contrast gratings that include some thousand periods, we can assume with high accuracy that the resonant coupling occurs only between the modes that satisfy the phase matching condition $k_n - k_m + Kl = 0$ (see the details below). In TFBGs considered here, the grating period is chosen to ensure resonant coupling between the core mode and the cladding modes (the appropriate variables will be labeled by subscripts c and n). The short-period (Bragg) gratings considered in the present review ensure resonance scattering of the core mode with $k_c > 0$ into the cladding mode with $k_n < 0$:

$$k_n = k_c - K , \tag{18}$$

which corresponds to the scattering of the core mode with $l = -1$ and the cladding mode with $l = 1$ in Eqns (17). By preserving only the resonant coupling, we get a system of equations for the modes of the core and the cladding:

$$\frac{2J_c}{c} \frac{\mathrm{d}a_c}{\mathrm{d}z} = \mathrm{i}k_0 \sum_n v_n a_n(z) \exp\left(-\mathrm{i}q_n z\right) , \tag{19}$$

$$\frac{2J_n}{c} \frac{\mathrm{d}a_n}{\mathrm{d}z} = \mathrm{i}k_0 v_n^* a_c(z) \exp\left(\mathrm{i}q_n z\right) , \tag{20}$$

where the coupling coefficients of the core and cladding modes are denoted as

$$v_n = \int \varepsilon_{-1} \mathbf{e}_c^* \mathbf{e}_n \, \mathrm{d}S , \tag{21}$$

$$v_n^* = \int \varepsilon_1 \mathbf{e}_c \mathbf{e}_n^* \, \mathrm{d}S , \tag{22}$$

and the detuning of wave numbers is denoted by $q_n = k_c - k_n + K$. To describe the Bragg peak among the cladding modes, it is necessary to consider the core mode propagating in the negative direction as well. System of equations (19), (20) describes a fiber with a tilted Bragg grating within the framework of the coupled mode theory.

Note that the resonant mode coupling under the phase matching condition is described by system of Eqns (19), (20). Let us integrate Eqn (20) from the beginning of the grating, $z = 0$, to its end, $z = L$. We take into account that the cladding mode appears due to the scattering of the core mode by the grating and travels in the opposite direction; as a result, the amplitude $a_n(z)$ is zero at the right-hand boundary of the grating:

$$a_n(0) = -\frac{\mathrm{i}ck_0 v_n^*}{2J_n} \int_0^L a_c(z') \exp\left(\mathrm{i}q_n z'\right) \mathrm{d}z' . \tag{23}$$

Since the oscillating factor $\exp\left(\mathrm{i}q_n z'\right)$ decreases the integral of the slowly changing amplitude $a_c(z')$, a resonance arises under the phase matching condition $q_n = 0$.

System (19), (20) allows describing both purely dielectric and plasmonic fiber sensors with tilted Bragg gratings. In the second case, the cladding modes should be calculated taking into account their hybridization with the plasmon of the metal layer.

Note that the magnitude of the transverse overlap integral (16) substantially depends on the grating tilt angle. In particular, for a nontilted grating, ε_1 is close to the permittivity inside the core; as a result, the overlap integral (16) is close to zero due to the orthogonality of the modes. On the other hand, in the presence of refractive index variations in the transverse section of the grating, this condition is substantially violated and mode coupling arises [48]. However, the presence of two–three cycles of refractive index in the transverse section does not allow speaking about transverse phase matching. To a certain degree of accuracy, it is possible to say that the grating tilt allows 'reflecting the mode from the core to the cladding.' The approximate character of the transverse phase matching gives rise to an envelope of the transmission spectrum [110, 112]. The solution of the system of equations describing the coupled modes is thoroughly studied in dissertation [112].

3. Methods of fabricating tilted Bragg gratings and sensors based on them

As mentioned in the Introduction, Bragg gratings are usually inscribed by radiation of UV laser [14, 26–28]. The methods of fabricating Bragg gratings can be conventionally divided into two types: inscribing by means of interferometers and using phase masks. The techniques of inscribing Bragg gratings by means of interferometers of different constructions are described in Refs [25, 114, 115]. Here, we will consider in more detail the inscription scheme using the phase mask [116], since the general principle of inscription is identical, but the use of a phase mask usually turns out to be a more practical method of TFBG fabrication.

The method of inscribing standard Bragg gratings using a phase mask is schematically illustrated in Fig. 9. The phase mask is a periodic structure in the form of lines in a plane. The lines are grooves of a specified depth, depending on the wavelength of the laser radiation used in the inscribing procedure. The grooves produce a phase shift of the wave passing through them by π with respect to the radiation passing through the main mass of the phase mask. This leads to the diffraction of the incident laser radiation with the dominant formation of the $+1$ and -1 diffraction orders and the subsequent formation of an interference pattern behind the mask plane due to their superposition. When a photosensitive optical fiber is placed in this region, the refractive index changes in the maxima of the interference pattern, thus forming the Bragg grating with a period equal to half a period of the phase mask (Fig. 9). Phase masks allow using relatively low-coherence radiation, e.g., that of excimer lasers. The method considered requires neither high temporal coherence nor spatial coherence, since, as a rule, the mask is installed in the immediate vicinity of the fiber.

The fixed phase mask period does not allow inscribing Bragg gratings for different wavelengths, which can be sometimes considered a drawback. On the other hand, the technique using phase masks is more reproducible and requires no complex schemes of vibroinsulation or stabilization of the optical scheme. This method is more practical in serial production of Bragg gratings and sensors based on them.

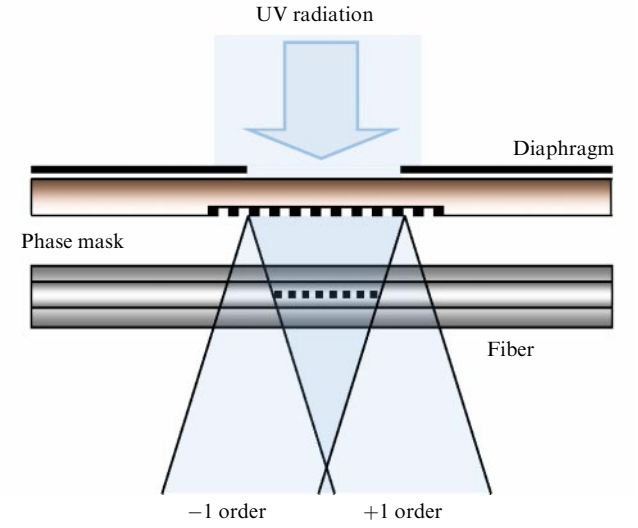

Figure 9. Method of Bragg grating inscription using a phase mask.

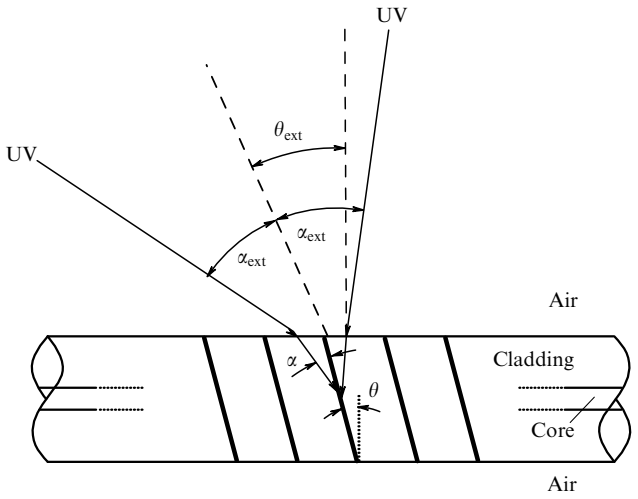

Figure 10. Principle of inscribing a TFBG by changing the angle of incidence of the radiation on the fiber [41].

The method of TFBG fabrication is based on creating a tilted interference pattern in the core of the optical waveguide. The tilt may be obtained using different incidence angles of the interfering beams to the optical waveguide surface. The principle of calculating the tilt angle of the resulting grating is clearly demonstrated in Fig. 10 [41].

The ultimate tilt angle of the grating can be calculated using the formula

$$\theta = \arcsin\left(\frac{\sin\theta_{ext}}{n}\right) \approx \frac{\theta_{ext}}{n}\,. \qquad (24)$$

In the case of inscribing a Bragg grating using a phase mask, such a tilt can be provided by rotating the mask–fiber system with respect to the direction of radiation incident on the mask (Fig. 11) [109].

An alternative version of inscription is to use a phase mask turned with respect to the fiber axis, as shown in Fig. 12 [109]. In this case, the axis of the fiber remains perpendicular to the axis of the laser optical radiation beam. Obviously, a similar inscription scheme can be implemented using spatial interferometers by appropriate rotation of the fiber with respect to the fringes of the interference pattern.

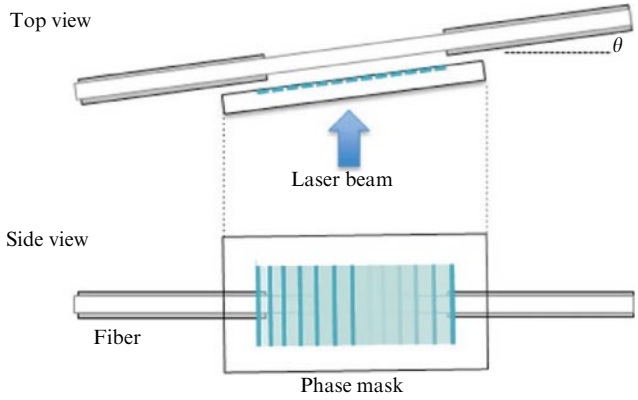

Figure 11. Inscribing a TFBG by rotating the mask–fiber system with respect to the radiation direction [109].

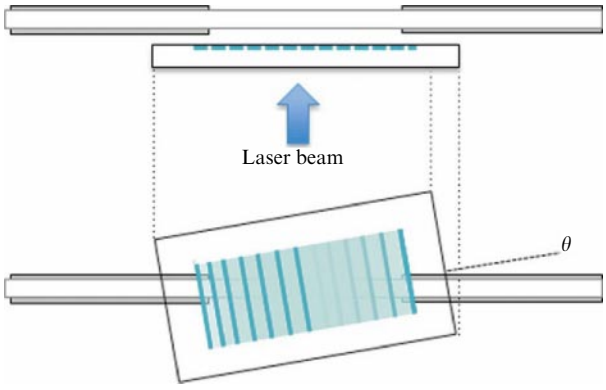

Figure 12. Inscribing a TFBG by rotating the mask with respect to the fiber waveguide axis [109].

Standard telecommunications, relatively low-doped optical fibers have low photosensitivity, which makes it difficult to inscribe Bragg gratings efficiently. To solve this problem, the method of high-pressure (100–150 atm) molecular hydrogen loading of fiber is often used. Under exposure to UV radiation, the hydrogen begins to interact with germanium present in the core of a telecommunications fiber, forming new centers that efficiently modify the mean refractive index of the exposed segment [117].

As noted in Section 2, in many cases, the side surface of the fiber should be functionalized to use the Bragg grating as a sensor. The role of functionalizing surface can be played by coatings sensitive to certain parameters of the environment, such as humidity, the presence of impurities, and gases. In the case of biosensors, antibodies to the detected antigens can serve as a functionalized surface. The range of surface functionalizing methods is extremely wide and depends on the type and material of the coating. However, the metallization of the outer surface of the fiber, which allows observing and using the effect of surface plasmon resonance in sensorics, deserves special consideration.

To fabricate plasmonic fiber sensors, it is necessary to apply a layer of metal, as a rule, gold, on a side surface of the fiber in the TFBG zone. Gold is a chemically inert material, which ensures the stability of sensor element operation for a long time. The typical thickness of the gold layer on the fiber surface, which ensures the most efficient coupling of the cladding modes with the plasmon in a plasmon sensor, is 35–50 nm. Typically, metal films of the specified thickness are

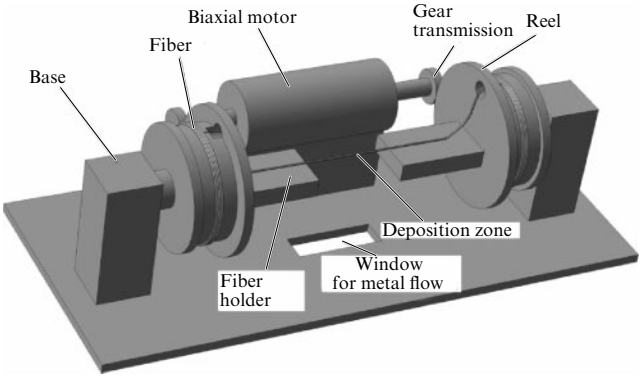

Figure 13. Schematic diagram of a rotating mechanism for coating a fiber with a metal layer.

deposited using magnetron or thermal sputtering in a vacuum. The target object for deposition is placed in the path of a flow of vaporized metal. However, in the case of a fiber, the layer should be applied to the side cylindrical surface. As a rule, this problem is solved by sequential deposition of the metal layer from two sides of the fiber [100]. The produced layer is rather nonuniform around the fiber and, in spite of demonstrating the capability of operation of plasmonic sensors with nonuniform coating in some papers [100], such technology substantially restricts the serial production of plasmonic TFBG-based sensors with reproducible characteristics.

The problem of uniform layer deposition can be solved by implementing an axial rotation of the fiber section above the metal evaporator. The Bragg grating can be located in the center of a long section of the optical fiber, which complicates the rotation task. The construction of a mechanism ensuring rotation was proposed in Refs [105, 107] (Fig. 13).

A biaxial motor is installed on the mechanism base that synchronously rotates two reels through a gear transmission. The reels are equipped with fiber holders. Such a mechanism is able to rotate a section of the fiber subjected to sputtering around its axis. The coated section can be in the center of a long part of the fiber. The fiber ends can be spooled on the side reels. The vaporized metal passes through a window in the bottom part of the base, under which the evaporators are located. The period of fiber rotation is much shorter than the time of metal evaporation, which ensures the deposition of a uniform layer on the fiber side surface.

4. Mathematical processing of fiber sensor spectra

When using TFBGs as sensitive elements of various sensors, the issue of the analysis of the grating spectral characteristics becomes relevant. Obviously, the sensor operation accuracy is directly related to the accuracy of this analysis. TFBG-based sensors have a rather complex transmission spectrum, and its mathematical processing is not trivial.

In the literature, there is a variety of approaches to the analysis of TFBG spectra. For example, in a number of papers, it is proposed that the fall in intensity of the cladding mode peaks with respect to a certain predetermined level be considered a cut-off indication [118] (Fig. 14). In this example, the crossing of the normalized spectrum and the constant level of 0.3 dB are accepted for the cut-off

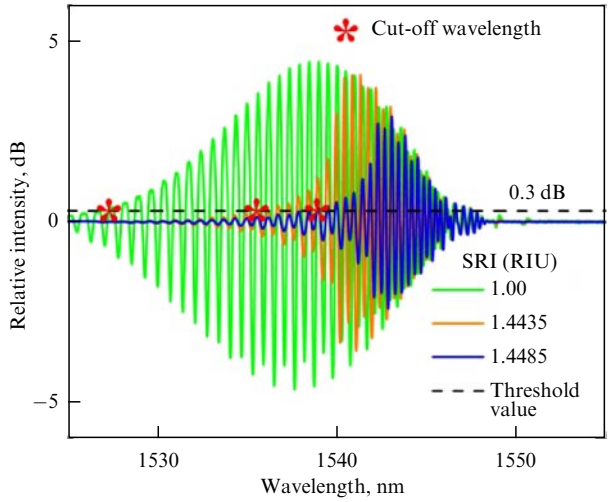

Figure 14. Determining the cut-off wavelength position from the intensity of spectral peaks [118]. SRI — surrounding refractive index, PIU refractive index unit.

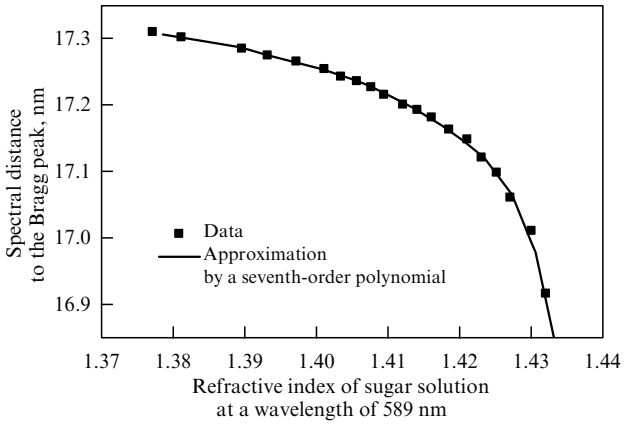

Figure 15. Separation between spectral peaks as a function of the surrounding refractive index [55].

wavelength position. The overall accuracy of the method has the order of 10^{-3} refractive index units (RIUs), reaching a level of 2.5×10^{-5} in the case of small changes. In this case, the sensitivity varies within the range from 300 to 100 nm RIU $^{-1}$.

Other authors use the change in the position of one or a few individual spectral peaks [55] (Fig. 15). Reference [118] investigates the dependence of the separation between one of the cladding-mode peaks and the Bragg peak on the external refractive index. The accuracy is declared to be at a level of 10^{-4} RIU, the method sensitivity being extremely low and nonlinear (from 20 to 3900 pm RIU $^{-1}$).

It should be kept in mind that such methods are not suitable as a universal algorithm for processing the indications of various sensors in various wavelength ranges. Moreover, their accuracy is substantially limited by the repetition rate and amplitude of peaks in the spectrum.

The technique proposed in Ref. [119] (Fig. 16) can be considered one of the most successful methods of processing signals from a TFBG-based refractometer. The method makes use of many spectral peaks, which allows achieving high measurement accuracy (to $\pm 5 \times 10^{-5}$). However, the method is rather complex and requires performing a laborious calibration procedure for each sensor sample. Moreover, the

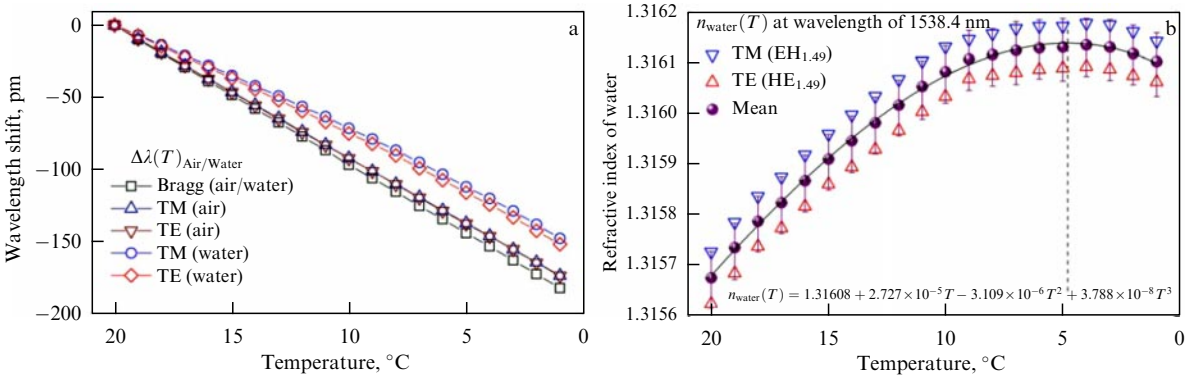

Figure 16. Results of processing the signal from a TFBG-based fiber refractometer by the example of measuring the refractive index of water upon a change in temperature: (a) spectral shifts of the Bragg peak and peaks corresponding to cladding modes, (b) dependence of the water refractive index on temperature [119].

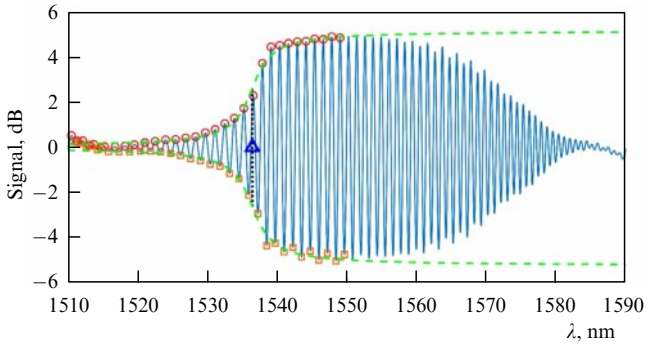

Figure 17. Using spectrum envelopes to search for the cut-off position [120].

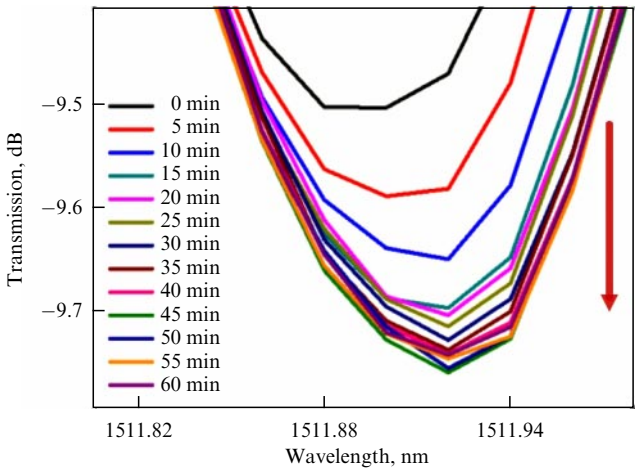

Figure 18. Processing the plasmonic sensor signal by measuring the amplitude of a separate spectral peak [97].

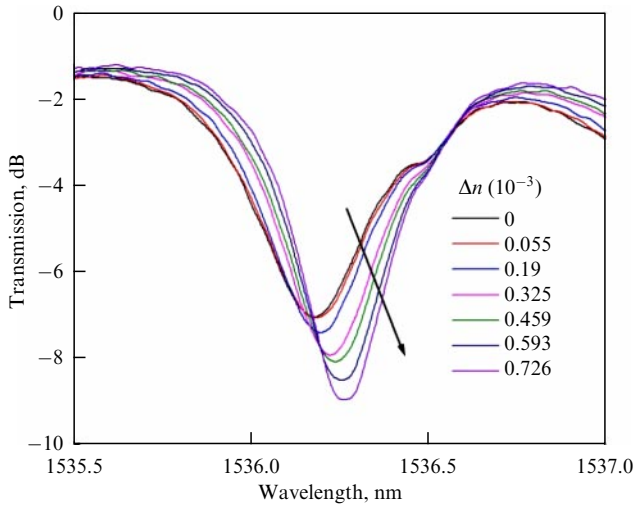

Figure 19. Processing the plasmonic sensor signal by measuring the amplitude and wavelength of a separate spectral peak [109].

method does not take into account the position of the cut-off, whose change is a much more noticeable effect than the shifts in the wavelengths of individual peaks used in Ref. [119].

Another successful method of processing the spectral characteristics may be to search for the cut-off position by constructing spectrum envelopes [120] (Fig. 17). The advantage of this approach is the use of a large amount of spectral information, whereas other algorithms deal only with particular parts of the spectrum. Naturally, the accuracy of this method is significantly higher and allows reaching the resolution at a level of 3.7×10^{-5} RIU in relative measurements, requiring no additional calibration procedure.

A separate problem is to analyze the spectra of plasmonic TFBG-based sensors. The transmission spectra of such sensors (see Fig. 8) have a rather complex structure with a variety of local extrema. However, none of these extrema is a direct manifestation of a resonance in the spectrum. On the contrary, the entire set of maxima points forms a pattern of the envelope characteristic, which is just what reacts to the change in the plasmon resonance position. For this reason, the determination of the position of resonance is a nontrivial problem that requires special consideration. As in the previous case, the accuracy of determining the resonance position in the fiber sensor spectrum will largely determine the accuracy of the sensor itself. For example, in Refs [97, 100, 109, 121–124], the main method of determining the resonance shift is the analysis of parameters of one or a few spectral peaks of the grating near the resonance wavelength. The measured parameters are the amplitude of a separate peak (Fig. 18) and its own position in the spectrum or both these parameters (Fig. 19). It is important to note that the main change in the above parameters is observed near the plasmon resonance [50]. The drawbacks of the method are the strong effect of noises on the analysis of an individual spectral peak, as well as the small value of the spectral shift, which does not allow performing the analysis with sufficiently high accuracy.

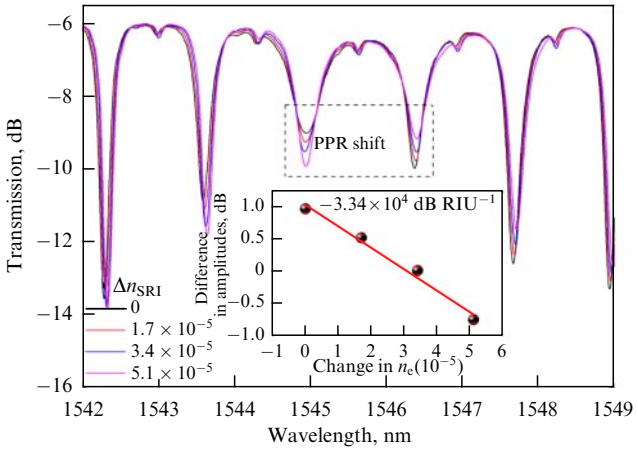

Figure 20. Estimation of surface plasmon resonance (SPR) shift by the differential amplitude change in two adjacent peaks [100].

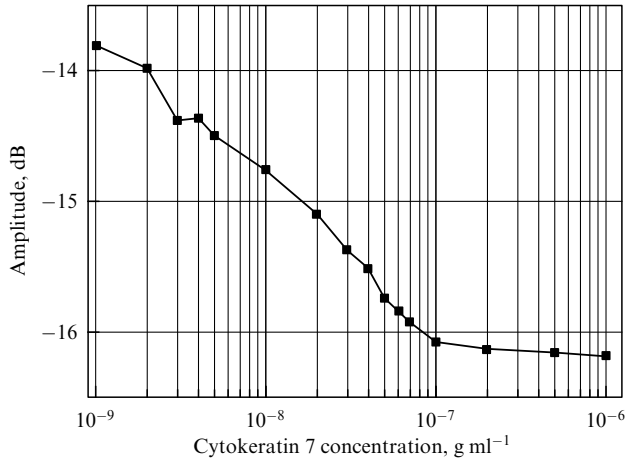

Figure 21. Dependence of the change in the amplitude of a separate peak on analyte concentration [122].

An improved version of the algorithm is the comparative analysis of intensities of two selected peaks (Fig. 20). In this case, the peaks with the greatest amplitude of change in the sensor working range, located on different sides of the spectral waist of the plasmon resonance, are chosen, which makes it possible to obtain the maximum slope of the sensor sensitivity characteristic, i.e., the maximal response to the change in the external medium parameters.

Indeed, with small changes in the external medium refractive index (not greater than 5×10^{-5}), the considered methods can ensure a relatively high resolution and detection limit, up to 3×10^{-6} [100, 109]. On the other hand, applying such methods to large refractive index changes can lead to significant errors, since it becomes necessary to consider other spectral peaks as the wavelength of the plasmon resonance changes. The sensitivity curve of the considered methods substantially differs from a linear dependence even in a small dynamic range (Fig. 21). Consequently, the monotonicity in the sensor indications is violated and the method itself does not appear to be universal.

Due to individual spectral characteristics of each sensor, the amplitude method of analysis requires individual calibration for each measurement range. Moreover, the limited accuracy and reproducibility of methods for determining intensities of individual spectral peaks can also be due to the

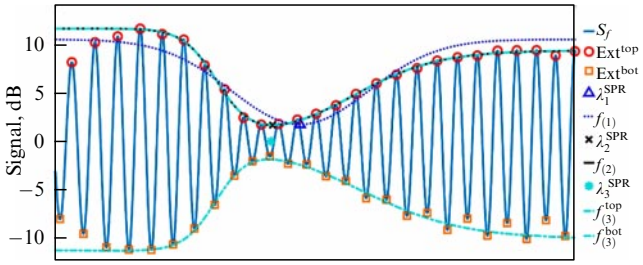

Figure 22. Analysis of the plasmonic sensor spectrum using envelopes [106]. Notations: S_f — spectral curve, Ext^{top} — top extrema, Ext^{bot} — bottom extrema, λ_1^{SPR} — estimate of the resonance position by method 1, envelope minimum number 1, $f_{(1)}$ — envelope number 1 (parabolic-type), λ_2^{SPR} — estimate of the resonance position by method 2, envelope minimum number 2, $f_{(2)}$ — envelope number 2 (6-parametric biexponential), λ_3^{SPR} — estimate of the resonance position by method 3, mean position of envelope extrema number 3, $f_{(3)}^{\text{top}}$ — top envelope number 3 (6-parametric biexponential), $f_{(3)}^{\text{bot}}$ — bottom envelope number 3 (6-parametric biexponential).

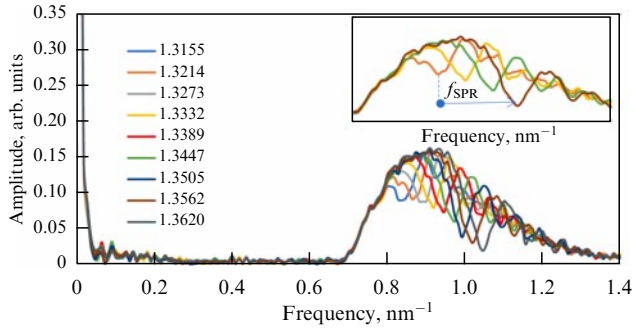

Figure 23. Fourier transform of the plasmonic sensor spectrum at different values of the external refractive index [125]; f_{SPR} — PPR frequency.

presence of spectral noises in both the source and the detector of the probing radiation.

Methods based on searching directly for the resonance region in the spectrum seem much more promising. One such method is based on the analysis of the spectrum envelopes with subsequent determination of the 'waist' position. For example, Ref. [106] analyzes the possibility of applying multiparametric curves followed by the search for their extrema. To normalize and reduce the spectral noises, the spectrum itself is subjected to preliminary bandpass filtering using the Fourier transform. The key feature of using the method of parametric curves is the analysis of the entire effective set of upper and lower maxima of the spectrum rather than one or two spectral peaks, which allows a substantial increase in the analysis accuracy (Fig. 22).

In the present case, the upper and lower envelopes are 6-parametric curves (turquoise curves in Fig. 22), approximating the set of local maxima (red circles) and minima (orange squares), respectively. The resonance position is accepted to be the wavelength, which is the average between the minimum of the upper envelope and the maximum of the lower envelope. Such an approach allows obtaining high resolution with respect to the refractive index of the external medium (about 3×10^{-6} RIU) within a wide range of measured values (not less than 5×10^{-2}).

Analyzing the Fourier transform of the spectrum and searching for the position of resonance directly on it seem to be yet other interesting solutions [125]. Indeed, since the characteristic 'waist' decreases the intensity of a few spectral peaks, and the peaks themselves in this case have a variable

repetition rate in the spectrum, the plasmon resonance will manifest itself as a characteristic spectral dip (Fig. 23).

Such a method of analysis seems promising thanks to using the entire array of spectral information, on the one hand, and the relative simplicity of the performed calculations, on the other hand.

5. Sensors based on tilted fiber Bragg gratings

The issue of using TFBG-based sensors in biosensorics deserves special attention. Ecology and medicine are becoming increasingly important in the modern world, which constantly increases requirements for the quantity and quality of measuring systems and instruments. Of particular popularity are biochemical plasmonic sensors used in immunoassays [49, 84, 92, 98, 105, 122, 126, 127]. In particular, there are many papers demonstrating the potential effectiveness of TFBG-based plasmonic sensors as biosensors, especially when the surface is functionalized with aptamers or antibodies [49, 109, 110, 122, 128, 129]. Based on planar schemes, such as Kretschmann's configuration, analytic complexes already exist and are being successfully used [81]. In the field of biosensorics development, fiber optics offers a number of fundamental advantages, such as compactness and mobility.

As a rule, biosensors are required to solve the problem of determining the presence and concentration of certain biomolecules in a solution. The principle of operation of most such sensors is based on the adsorption of biomolecules on a sensitive surface, which changes the local refractive index near the sensor surface. The sensor surface may be functionalized with antibodies or aptamers, which specifically attach the molecules of a certain analyte [122, 130]. As a result, being deposited into a biological solution, this sensor will adsorb only the desired biomolecules on its surface (Fig. 24).

As a rule, the process of active adsorption of biomolecules on a sensor surface takes some time (a few minutes, rarely a few ten minutes). After filling the entire active surface, the process saturates and the sensor signal tends to a new constant level. The time to become established at this new level can correlate with the level of concentration of biomolecules in the solution, which can be used to determine this concentration [97, 105, 109]. For example, in Ref. [97], the level of concentration of the aquaporin-2 (AQP2) protein, a biomarker of kidney diseases, was studied. The sensor surface was functionalized with appropriate antibodies. In sick rats, the level of protein in their urine was higher, which manifested itself in indications of the plasmonic sensor (Fig. 25, red curve). In Ref. [109], the surface functionalization was implemented by means of aptamers specific to thrombin. In the reaction of the sensor to the thrombin concentration at a level of 5 μM in a solution, similar dynamics are observed with a characteristic time of the order of 10 min [109] (Fig. 26). Reference [105] shows the correlation between the plasmonic sensor response time and the concentration of the solution.

The possibility of incorporating a fiber biosensor into the channel of a microfluidic chip opens up broad prospects. The chip itself is a small-sized cell made of a chemically inert material with narrow channels that ensure the flow of the investigated liquid. The development of such cells was inspired by the popular lab-on-a-chip concept, which consists of carrying out all the necessary measurements in a single miniature device that does not require large volumes of the initial analyte (several microliters). Figure 27 schematically shows a microfluidic chip with an embedded fiber sensor.

Such designs make it possible to ensure the movement of the liquid under study, to protect the measurement area from the influence of the external environment, while fixing the

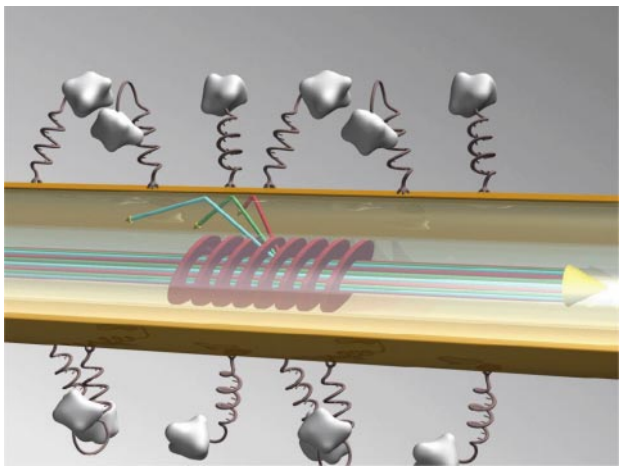

Figure 24. Principle of operation of a biosensor functionalized surface [109].

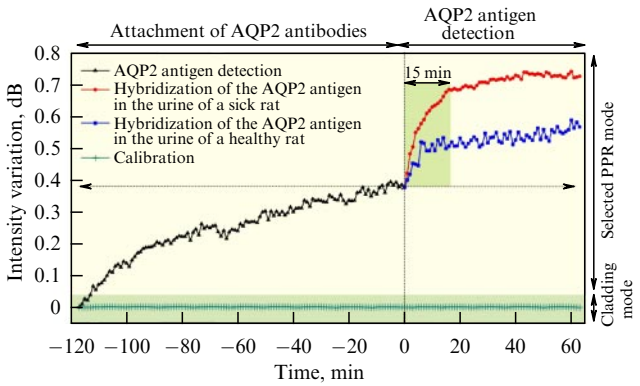

Figure 25. Result of the process of functionalization of the surface and adsorption of biomolecules on a sensor surface in the form of time dependence [97].

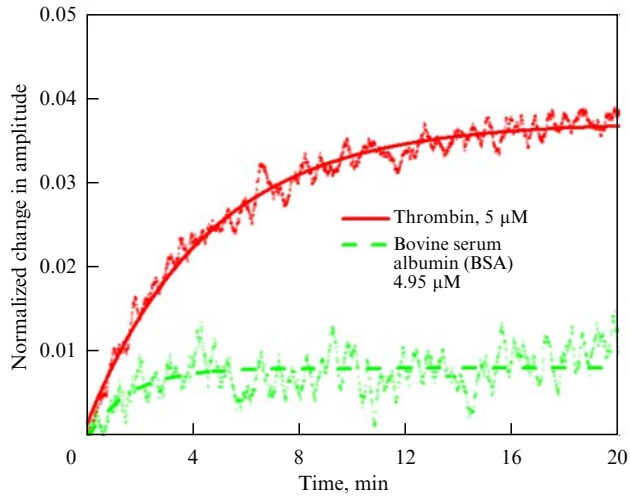

Figure 26. Result of the process of adsorption of biomolecules on a sensor surface in the form of a time dependence [109].

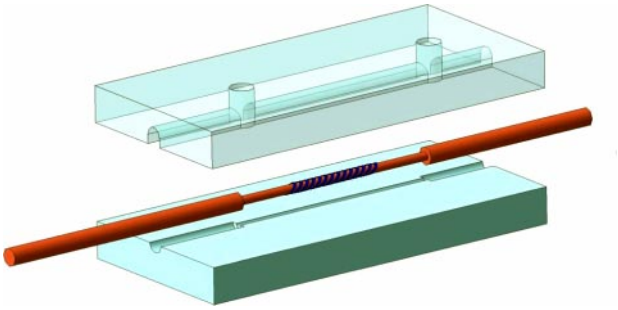

Figure 27. Schematic representation of a microfluidic chip with a built-in fiber sensor [53].

sensitive element itself and reducing the likelihood of introducing errors associated with polarization instability.

6. Conclusion

The development of fiber optic architecture requires the integration of various devices into optical fibers. Sensors are an important class of such devices. This review describes fiber sensors based on tilted Bragg gratings. Such structures make it possible to provide a well-controlled interaction of the fundamental fiber mode with cladding modes, whose properties depend on the environmental parameters.

Highly sensitive plasmonic sensors based on tilted Bragg gratings are being actively studied. Functionalization of the surface of such sensors can significantly expand the range of their applications. In particular, the development of TFBG-based chemical and physical sensors, sensors for detecting biological objects in analytes, and immunoassay systems is being actively pursued.

To date, the manufacture of tilted Bragg gratings has been mastered at a high level. However, for commercial implementations of BG-based fiber sensors, it is necessary to solve a number of problems, including the ensured stability of the parameters of these structures, as well as improving the methods for processing the output data, i.e., the complex transmission spectrum of such a sensor. Thus, a number of algorithms have already been proposed for processing signals from a TFBG-based sensor, which allow appropriate recognition of certain features in the transmission spectrum: the cut-off wavelength, the spectral envelope describing the plasmon resonance, and the frequency shifts of cladding modes. By now, there is an awareness of the importance of using mighty processing algorithms in the analysis of data from various optical sensors. Rigid requirements for the accuracy and complexity of the processed data necessitate the use of neural networks and machine learning methods [131, 132]. Further research on fiber sensors based on TFBGs will probably move in this direction.

Acknowledgments. This study was supported by the Russian Foundation for Basic Research (project no. 20-17-50123).

References

1. Kapron F P, Keck D B, Maurer R D *Appl. Phys. Lett.* **17** 423 (1970)
2. Gulyaev Yu et al. *Foton-Express* (6) 114 (2005)
3. Zheltikov A M *Phys. Usp.* **43** 1125 (2000); *Usp. Fiz. Nauk* **170** 1203 (2000)
4. Zheltikov A M *Phys. Usp.* **50** 705 (2007); *Usp. Fiz. Nauk* **177** 737 (2007)
5. Dianov E M, Kryukov P G *Quantum Electron.* **31** 877 (2001); *Kvantovaya Elektron.* **31** 877 (2001)
6. Voloshin V V et al. *J. Commun. Technol. Electron.* **54** 847 (2009); *Radiotekhnika Elektron.* **54** 890 (2009)
7. Popov S M et al. *Quantum Electron.* **49** 1127 (2019); *Kvantovaya Elektron.* **49** 1127 (2019)
8. Butov O V, Dianov E M, Golant K M *Meas. Sci. Technol.* **17** 975 (2006)
9. Ramakrishnan M et al. *Sensors* **16** 99 (2016)
10. Ye X W, Su Y H, Han J P *Sci. World J.* **2014** 652329 (2014)
11. Yatseev V A, Zotov A M, Butov O V *Results Phys.* **19** 103485 (2020)
12. Tomyshev K A et al. *Proc. SPIE* **10323** 103235K (2017)
13. Dianov E M *Phys. Usp.* **47** 1065 (2004); *Usp. Fiz. Nauk* **174** 1139 (2004)
14. Kashyap R *Fiber Bragg Gratings* (Burlington, MA: Academic Press, 2010)
15. Wikszak E et al. *Opt. Lett.* **31** 2390 (2006)
16. Bagan V A, Nikitov S A, Chamorovsky Yu K *Usp. Sovrem. Radioelektron.* (5) 65 (2010)
17. Smirnov A M et al. *ACS Photon.* **5** 5038 (2018)
18. Butov O V et al. *J. Opt. Soc. Am. B* **34** A43 (2017)
19. Rybaltovsky A A et al. *Results Phys.* **16** 102832 (2020)
20. Smirnov A M, Butov O V *Opt. Lett.* **46** 86 (2021)
21. Nechepurenko I A, Dorofeenko A V, Butov O V *Opt. Express* **29** 13657 (2021)
22. Popov S M et al. *Results Phys.* **9** 806 (2018)
23. Hill K O et al. *Appl. Phys. Lett.* **32** 647 (1978)
24. Bragg W L *Scientia* **23** 153 (1929)
25. Meltz G, Morey W W, Glenn W H *Opt. Lett.* **14** 823 (1989)
26. Othonos A *Rev. Sci. Instrum.* **68** 4309 (1997)
27. Vasil'ev S A et al. *Quantum Electron.* **35** 1085 (2005); *Kvantovaya Elektron.* **35** 1085 (2005)
28. Hill K O, Meltz G *J. Lightwave Technol.* **15** 1263 (1997)
29. Butov O V et al. *Zh. Priklad. Spektrosk.* **83** (6-16) 661 (2016)
30. Krohn D A, MacDougall T, Mendez A *Fiber Optic Sensors: Fundamentals and Applications* (Bellingham, WA: SPIE Press, 2014)
31. Butov O V et al. *Sensors* **19** 4228 (2019)
32. Butov O et al., in *Optical Fiber Sensors. Proc. TuB6 Optical Society of America* (2006)
33. Butov O V et al. *Proc. SPIE* **9157** 91570X (2014)
34. Rao Y-J *Opt. Lasers Eng.* **31** 297 (1999)
35. Moyo P et al. *Eng. Struct.* **27** 1828 (2005)
36. Qiao X et al. *Sensors* **17** 429 (2017)
37. Kinet D et al. *Sensors* **14** 7394 (2014)
38. Ivanov O V, Nikitov S A, Gulyaev Yu V *Phys. Usp.* **49** 167 (2006); *Usp. Fiz. Nauk* **176** 175 (2006)
39. Meltz G, Morey W, Glenn W, in *Optical Fiber Communication Conf.. Proc. TUG1 Optical Society of America* (1990)
40. Kashyap R, Wyatt R, Campbell R *Electron. Lett.* **29** 154 (1993)
41. Erdogan T, Sipe J E *J. Opt. Soc. Am. A* **13** 296 (1996)
42. Liu Y, Zhang L, Bennion I *Meas. Sci. Technol.* **10** L1 (1999)
43. Lee K S, Erdogan T *Appl. Opt.* **39** 1394 (2000)
44. Li Y, Froggatt M, Erdogan T *J. Lightwave Technol.* **19** 1580 (2001)
45. Westbrook P, Strasser T, Erdogan T *IEEE Photon. Technol. Lett.* **12** 1352 (2000)
46. Zhou K et al. *Opt. Lett.* **30** 1285 (2005)
47. Mihailov S et al. *Electron. Lett.* **37** 284 (2001)
48. Albert J, Shao L Y, Caucheteur C *Laser Photon. Rev.* **7** 83 (2013)
49. Caucheteur C, Guo T, Albert J *Analyt. Bioanalyt. Chem.* **407** 3883 (2015)
50. Caucheteur C et al. *Opt. Express* **19** 1656 (2011)
51. Dong X et al. *Photon. Sensors* **1** 6 (2011)
52. Chiu Y-D, Wu C-W, Chiang C-C *Sensors* **17** 2129 (2017)
53. Tomyshev K A et al. *Phys. Status Solidi A* **216** 1800541 (2019)
54. Dolzhenko E I, Tomyshev K, Butov O V *Proc. SPIE* **11772** 117720S (2021)
55. Chan C-F et al. *Appl. Opt.* **46** 1142 (2007)
56. Laffont G, Ferdinand P *Meas. Sci. Technol.* **12** 765 (2001)
57. Guo T et al. *Opt. Express* **17** 5736 (2009)
58. Miao Y-p, Liu B *Opt. Fiber Technol.* **15** 233 (2009)
59. Cai Z et al. *Opt. Express* **23** 20971 (2015)
60. Zheng J et al. *Opt. Commun.* **312** 106 (2014)
61. Caucheteur C et al., in *Proc. SPIE* **5855** 451 (2005)

62. Giles C *J. Lightwave Technol.* **15** 1391 (1997)
63. Yariv A, Yeh P *Optical Waves in Crystals* (New York: Wiley, 1984); Translated into Russian: *Opticheskie Volny v Kristallakh* (Moscow: Mir, 1987)
64. Butov O V et al. *Opt. Commun.* **213** 301 (2002)
65. Hale G M, Querry M R *Appl. Opt.* **12** 555 (1973)
66. Sypabekova M et al. *Biosensors Bioelectron.* **146** 111765 (2019)
67. Miao Y et al. *IEEE Photon. Technol. Lett.* **21** 441 (2009)
68. Dolzhenko E I, Tomyshev K, Butov O V *Phys. Status Solidi RRL* **14** 2000435 (2020)
69. Aldaba A L et al. *Sensors Actuators B* **254** 1087 (2018)
70. Maier S A *Plasmonics: Fundamentals and Applications* (New York: Springer, 2007)
71. Brongersma M L, Kik P G *Surface Plasmon Nanophotonics* (New York: Springer, 2007)
72. Sarid D, Challener W A *Modern Introduction to Surface Plasmons: Theory, Mathematica Modeling and Applications* (Cambridge: Cambridge Univ. Press, 2010)
73. Astapenko V A *Elektromagnitnye Protsessy v Srede, Nanoplazmonika i Metamaterialy* (Electromagnetic Processes in Matter, Nanoplasmonics and Metamaterials) (Dolgoprudnyi: ID Intellekt, 2012)
74. Kretschmann E, Raether H *Z. Naturforschung A* **23** 2135 (1968)
75. Agranovich V M, Mills D L *Surface Polaritons: Electromagnetic Waves at Surfaces and Interfaces* (Amsterdam: North-Holland, 1982)
76. Raether H *Surface Plasmons on Smooth and Rough Surfaces and on Gratings* (Berlin: Springer, 1988)
77. Shalaev V M, Kawata S (Eds) *Nanophotonics with Surface Plasmons* (Advances in Nano-Optics and Nano-Photonics, Vol. 2) (Amsterdam: Elsevier, 2007)
78. Vinogradov A P et al. *Phys. Rev. B* **97** 235407 (2018)
79. Homola J, Yee S S, Gauglitz G *Sensors Actuators B* **54** 3 (1999)
80. Homola J, Piliarik M, in *Surface Plasmon Resonance Based Sensors* (Ed. J Homola) (Berlin: Springer, 2006) p. 45
81. Rich R L, Myszka D G *J. Mol. Recognition* **18** 431 (2005)
82. Naimushin A N et al. *Biosensors Bioelectron.* **17** 573 (2002)
83. Nechepurenko I A et al. *Zh. Radioelektron.* (4) 1 (2015); http://jre.cplire.ru/jre/apr15/11/text.pdf
84. Lin H-Y et al. *Sensors Actuators A* **138** 299 (2007)
85. Gentleman D J, Booksh K S *Talanta* **68** 504 (2006)
86. Dwivedi Y S, Sharma A K, Gupta B D *Plasmonics* **3** 79 (2008)
87. Lin H-Y et al. *Opt. Express* **20** 21693 (2012)
88. Navarrete M-C et al. *Sensors Actuators B Chemical* **190** 881 (2014)
89. Verma R K, Sharma A K, Gupta B D *Opt. Commun.* **281** 1486 (2008)
90. Iga M, Seki A, Watanabe K *Sensors Actuators B* **101** 368 (2004)
91. Takagi K et al. *Sensors Actuators A* **161** 1 (2010)
92. Lin Y et al. *Sensors* **10** 9397 (2010)
93. Nguyen H et al. *Appl. Phys. Lett.* **103** 193116 (2013)
94. Consales M et al. *ACS Nano* **6** 3163 (2012)
95. Jeong H-H et al. *Opt. Eng.* **50** 124405 (2011)
96. Sai V V R, Kundu T, Mukherji S *Biosensors Bioelectron.* **24** 2804 (2009)
97. Han L et al. *J. Lightwave Technol.* **35** 3360 (2017)
98. Marquez-Cruz V, Albert J *J. Lightwave Technol.* **33** 3363 (2015)
99. Baiad M D et al. *Opt. Lett.* **38** 4911 (2013)
100. Feng D et al. *Opt. Express* **24** 16456 (2016)
101. Shao L-Y, Shevchenko Y, Albert J *Opt. Express* **18** 11464 (2010)
102. Shevchenko Y Y, Albert J *Opt. Lett.* **32** 211 (2007)
103. Caucheteur C, Voisin V, Albert J *Opt. Express* **21** 3055 (2013)
104. Voisin V et al. *Appl. Opt.* **50** 4257 (2011)
105. Tomyshev K A et al. *J. Appl. Phys.* **124** 113106 (2018)
106. Manuylovich E, Tomyshev K, Butov O V *Sensors* **19** 4245 (2019)
107. Tomyshev K, Tazhetdinova D, Butov O, in *2017 Progress in Electromagnetics Research Symp.-Spring* (*PIERS*) (2017)
108. Ortega-Gomez A et al. *Opt. Express* **29** 18469 (2021)
109. Albert J et al. *Methods* **63** 239 (2013)
110. Guo T et al. *Biosensors Bioelectron.* **78** 221 (2016)
111. Snyder A W *J. Opt. Soc. Am.* **62** 1267 (1972)
112. Bialiayeu A "Tilted fibre Bragg grating sensors with resonant nanoscale coatings. Simulation of optical properties", Doctoral Thesis (München: GRIN Verlag, 2015)
113. Chen C-L *Foundations for Guided-Wave Optics* (Hoboken, NJ: Wiley-Interscience, 2007)
114. Patrick H, Gilbert S L *Opt. Lett.* **18** 1484 (1993)
115. Askins C G et al. *Opt. Lett.* **19** 147 (1994)
116. Hill K O et al. *Appl. Phys. Lett.* **62** 1035 (1993)
117. Lemaire P J et al. *Electron. Lett.* **29** 1191 (1993)
118. Pham X et al. *J. Appl. Phys.* **123** 174501 (2018)
119. Zhou W, Zhou Y, Albert J *Laser Photon. Rev.* **11** 1600157 (2017)
120. Tomyshev K et al. *Sensors Actuators A* **308** 112016 (2020)
121. Yuan Y et al. *Analyt. Chem.* **88** 7609 (2016)
122. Ribaut C et al. *Biosensors Bioelectron.* **77** 315 (2016)
123. Ribaut C et al. *Biosensors Bioelectron.* **92** 449 (2017)
124. Shevchenko Y et al. *Opt. Lett.* **35** 637 (2010)
125. Udos W et al. *Optik* **219** 164970 (2020)
126. Cao Y et al. *Appl. Spectrom. Rev.* **50** 499 (2015)
127. Riboh J C et al. *J. Phys. Chem. B* **107** 1772 (2003)
128. Lobry M et al. *Biomed. Opt. Express* **11** 4862 (2020)
129. Leitão C et al. *IEEE Sensors J.* **21** 3028 (2020)
130. Ricciardi A et al. *Analyst* **140** 8068 (2015)
131. Kornienko V V et al. *IEEE Sensors J.* **20** 6954 (2020)
132. Chubchev E D et al. *J. Lightwave Technol.* **40** 3046 (2022)